# Supporting Information

## Visible-range hemi-indigo photoswitch: ON-OFF fluorescent binder for HIV-1 RNA

Daria V. Berdnikova*†

†Universität Siegen, Organische Chemie II, Adolf-Reichwein-Str. 2, 57076 Siegen, Germany

Table of Contents:

## 1. Materials and equipment

**Reagents and solvents** were obtained from commercial sources (Acros, Merck, Fischer) and used as received. Reactions were monitored on POLYGRAM® SIL G/$UV_{254}$ (Macherey-Nagel) TLC plates with detection by UV light irradiation (254 nm or 366 nm). Column chromatography was performed on cellulose microcrystalline (Alfa Aesar) and Sephadex® columns.

**$^{1}$H NMR and $^{13}$C NMR spectra** were recorded on *Brucker 400* and *Varian VNMR-S 600* spectrometers at 25 °C using 5 mm or 3 mm tubes. Chemical shifts were determined with accuracy of 0.01 ppm and 0.1 ppm for $^{1}$H and $^{13}$C spectra, respectively, and are given relative to the residual signal of the solvent that was used as internal standard ($CDCl_3$: $\delta_H$ = 7.27 ppm; acetone-$d_6$: $\delta_H$ = 2.05 ppm, $\delta_C$ = 29.8 ppm). Spin–spin coupling constants for the proton spectra were determined with accuracy of 0.2 Hz. The proton NMR signal assignments were performed using COSY and ROESY 2D NMR techniques. The carbon NMR signal assignments were performed by means of HSQC and HMBC 2D NMR techniques.

**Electrospray ionization (ESI) mass spectra** were recorded on a *Finnigan LCQ Deca* mass-spectrometer.

**Elemental analysis** was performed with a *HEKAtech EUROEA* combustion analyser by Mr. Rochus Breuer (Universität Siegen, Organische Chemie I).

**Melting points** were measured with a *BÜCHI 545* (BÜCHI, Flawil, CH) melting point apparatus in open capillaries and are uncorrected.

**Electronic absorption spectra** were measured on a *Cary 100 Bio* two-beam spectrophotometer. Thermal relaxation kinetics and photoisomerization quantum yields were measured on a *Specord 600* (Analytik Jena AG) diode-array spectrophotometer.

**Fluorescence spectra** were recorded on a *Cary Eclipse* spectrofluorimeter.

**Circular dichroism spectra** were measured with an *Applied Photophysics Chirascan* CD spectrometer.

**Optical spectroscopy measurements** were performed in thermostated quartz sample cells of 10 mm pathlength. Preparation and handling of the solutions were carried out under red light.

**Photochemical reactions** were performed using the following LED light sources: *Roschwege* Star-UV365-01-00-00 (365 nm); *Roithner* H2A1-H420 130 mW (420 nm); *Roschwege* HighPower-LED Blau (470 nm); *Roschwege* HighPower-LED Grün (520 nm); *Roschwege* HighPower-LED Amber (590 nm). Preparation and handling of the solutions were carried out under red light.

**Buffer solutions** for RNA studies were prepared from purified water (resistivity 18 MΩ $cm^{-1}$) and biochemistry-grade chemicals. A 10 mM Na-phosphate buffer (pH 7.0) containing 0.1 M NaCl (and

1 mM EDTA in the case of photometric and fluorimetric titrations) was used. Prior to use, the buffer was filtered through a PVDF membrane filter (pore size 0.45 μm) and autoclaved. All materials used for the RNA studies were RNase free. HIV-1 TAR RNA sequence [5′-GGCAGAUCUGAGCCUGGGAGCUCUCUGCC-3′] and HIV-1 RRE-IIB RNA sequence [5’-GGUCUGGGCGCAGCGCAAGCUGACGGUACAGGCC-3’] were purchased from *Biomers.net GmbH* (Ulm, Germany). HIV-1 Tat peptide (47–57) was purchased from *Merck*.

## 2. Synthesis

### 4-(3-(dimethylamino)propoxy)-3-methoxybenzaldehyde hydrochloride (2)

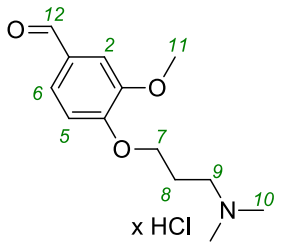


Vanillin (1.00 g, 6.57 mmol) and $K_2CO_3$ (1.2 eq., 1.25 g, 7.89 mmol) were suspended in 4 mL of dry DMF, flushed by argon and heated at 120 °C upon vigorous stirring for 1 h. Then the suspension of 3-dimethylamino-1-propyl chloride hydrochloride (2.5 eq., 2.27 g, 16.4 mmol) in 3 mL of dry DMF was added, the system was provided by a constant argon flow and stirred at 120 °C for 4.5 h. After this, the mixture was cooled down and stirred at ambient temperature for 22 h. The reaction was quenched by addition of $H_2O$ and extracted with $CH_2Cl_2$. The combined organic phase was dried over $Na_2SO_4$ and filtered off. Then 4 mL of 4M HCl solution in dioxane was added and the solvent was removed *in vacuo* to yield the desired product **2** as beige powder. The purity was good enough to use the product for the next step without further purification.

Yield 85% (1.53 g, 5.58 mmol). $^1$H NMR (400 MHz, $CDCl_3$, $\delta$ ppm, $J$ Hz): 2.47 (m, 2H, H-8); 2.88 (m, 6H, H-10); 3.31 (m, 2H, H-9); 3.89 (s, 3H, H-11); 4.24 (m, 2H, H-7); 6.99 (d, 1H, H-5, $J$ = 7.9); 7.39 (d, 1H, H-2, $J$ = 1.8); 7.43 (dd, 1H, H-6, $J$ = 7.9, 1.8); 9.84 (s, 1H, H-12).[1]

### (*Z*)-2-(4-(3-(dimethylamino)propoxy)-3-methoxybenzylidene)indolin-3-one (1)

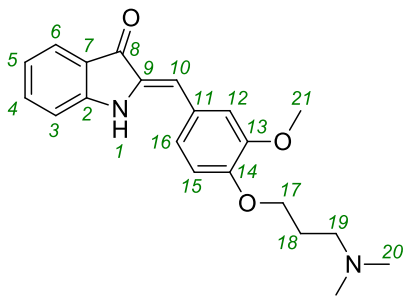


Dry indoxyl-3-acetate (0.050 g, 0.285 mmol) and 4-(3-(dimethylamino)propoxy)-3-methoxybenzaldehyde **2** (0.078 mg, 0.285 mmol) were placed in a two-neck round bottom flask and flushed with argon. After flushing, the flask was sealed by a septum and a constant argon flow was established. An argon-degassed solution of NaOH (0.080 mg, 2.00 mmol) in 6 mL of EtOH was injected into the flask through the septum under vigorous stirring. The mixture was stirred at r.t. for 2 h. Then the mixture was quenched by $H_2O$ and extracted by ethyl acetate. The solvent was removed and the residue was purified by column chromatography on cellulose (eluent: hexane–EtOAc going from 100:1 to 1:3). The product-enriched fraction was collected and purified two times by gel-filtration chromatography on sephadex (MeOH). The desired product **1** was isolated in pure *Z*-form as dark orange glass.

Yield 24% (0.024 mg, 0.068 mmol), $R_f$ = 0.07 (EtOH). $^1$H NMR (600 MHz, acetone-$d_6$, $\delta$ ppm, $J$ Hz): 1.92 (quint, 2H, H-18, $J$ = 6.8); 2.17 (s, 6H, H-20); 2.41 (t, 2H, H-19, $J$ = 7.0); 3.90 (s, 3H, H-21); 4.09 (t, 2H, H-17, $J$ = 6.4); 6.69 (s, 1H, H-10); 6.94 (t, 1H, H-5, $J$ = 7.6, 7.2); 7.02 (d, 1H, H-15, $J$ = 8.4); 7.15 (d, 1H, H-3, $J$ = 8.0); 7.28 (d, 1H, H-12, $J$ = 2.0); 7.30 (dd, 1H, H-16, $J$ = 8.0, 2.0); 7.48 (ddd, 1H, H-4, $J$ = 8.4, 7.1, 1.4); 7.62 (d, 1H, H-6, $J$ = 7.6); 8.92 (s, 1H, H-1). $^{13}$C NMR (151 MHz, acetone-$d_6$, $\delta$ ppm): 28.4 (1C, C-18); 45.8 (2C, C-20); 56.5 (1C, C-21); 56.9 (1C, C-19); 67.8 (1C, C-17); 111.8 (1C, C-10); 113.5 (1C, C-3); 114.3 (1C, C-15); 114.9 (1C, C-12); 120.7 (1C,

C-5); 122.3 (1C, C-7); 124.1 (1C, C-16); 124.8 (1C, C-6); 128.5 (1C, C-11); 135.0 (1C, C-9); 136.6 (1C, C-4); 150.6 (1C, C-14); 150.8 (1C, C-13); 155.0 (1C, C-2); 186.9 (1C, C-8). Elem. anal. calcd. (%) for $C_{21}H_{24}N_2O_3$: C, 71.57; H, 6.86; N, 7.95; found: C, 71.72; H, 6.73; N, 7.78. ESI-MS **1** in MeOH, *m/z*: calcd. 352.43; found 353.24 $[\mathbf{1}+H]^+$.

## 3. Optical spectroscopy studies

### *3.1. Photoswitching of hemi-indigo 1 in water at different irradiation wavelengths*

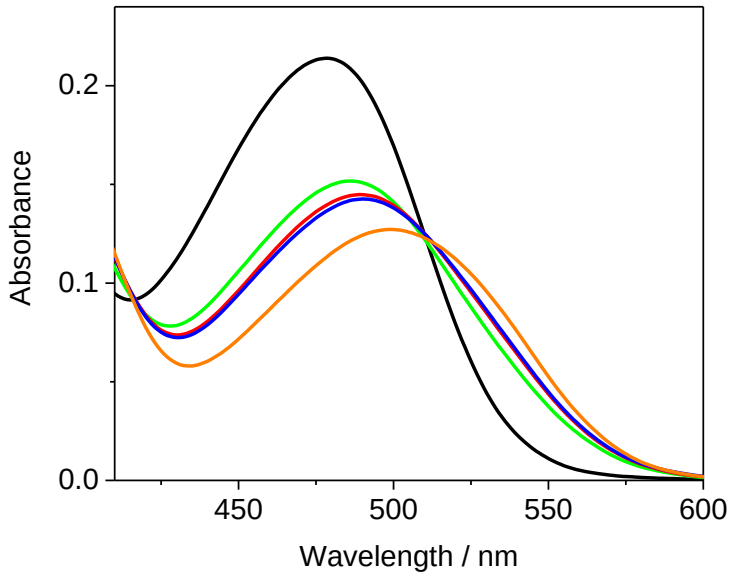


**Figure S1.** Absorption spectra of *Z*-**1** (black) and photostationary mixtures of *Z*- and *E*-isomers of **1** obtained upon irradiation with 365 nm (red), 420 nm (blue), 470 nm (orange) and 520 nm (green) light in water, $c$ = 20 μM.

### *3.2. Formation of the ternary associate 1–Tat–TAR*

To clarify whether *Z*-**1** can compete with Tat peptide for the TAR binding site or whether the triple complex **1**–Tat–TAR is formed the changes of the emission of the **1**–TAR complex were monitored upon addition of the Tat peptide (Figure S2). Considering that the association constant of Tat–TAR complex is two orders of magnitude larger than that of **1**–TAR complex,[2] the peptide should displace the ligand either directly or through the allosteric mechanism. However, the experiment showed only a slight decrease of the **1**–TAR emission intensity till the amount of Tat added reached 0.75 eq. and further changes were not detected. This indicates that the binding of the Tat peptide to TAR does not lead to a significant displacement of the ligand from the TAR, i. e. the triple complex **1**–Tat–TAR is formed with high probability. An additional experiment showed that the *Z*-isomer of hemi-indigo **1** does not interact with Tat protein in the absence of RNA (Figure S4A). Similar studies with the photostationary mixture in $PSS^{470}$ enriched with *E*-isomer (Figure S3) showed no displacement of the *E*-isomer by Tat from TAR RNA and no interaction of the *E*-isomer with Tat in the absence of RNA (Figure S4B).

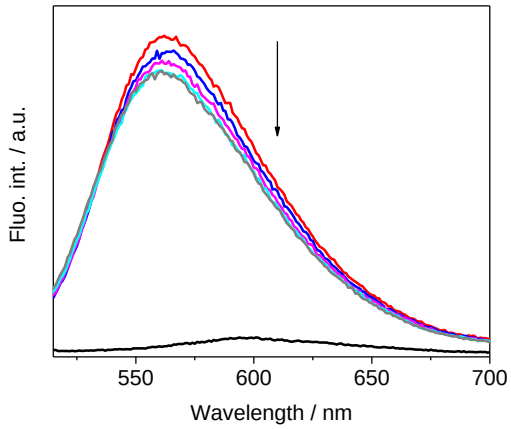


**Figure S2.** Fluorescence spectra of free *Z*-**1** (black) and *Z*-**1** in the presence of 1 eq. of TAR RNA (red) as well as changes of the emission of the **1**–TAR complex upon addition of Tar peptide; aliquots of Tat: 0.25 eq. (blue), 0.50 (magenta), 0.75 eq. (cyan), 1 eq. (grey). In all cases: $c_1$ = 10 μM, 10 mM Na-phosphate buffer with 0.1 M NaCl, pH = 7.0, $\lambda_{ex}$ = 496 nm, 20 °C. After addition of every Tat aliquote, the solution was thoroughly mixed and incubated for 10 min.

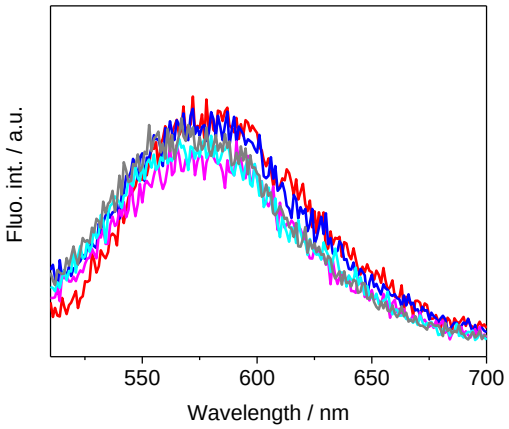


**Figure S3.** Fluorescence spectra of the photostationary mixture of *Z*- and *E*-isomers (20/80) of **1** in the presence of 1 eq. of TAR RNA (red) as well as changes of the emission upon addition of Tar peptide; aliquots of Tat: 0.25 eq. (blue), 0.50 (magenta), 0.75 eq. (cyan), 1 eq. (grey). In all cases: $c_1$ = 10 μM, 10 mM Na-phosphate buffer with 0.1 M NaCl, pH = 7.0, $\lambda_{ex}$ = 496 nm, 20 °C. After addition of every Tat aliquote, the solution was thoroughly mixed and incubated for 10 min.

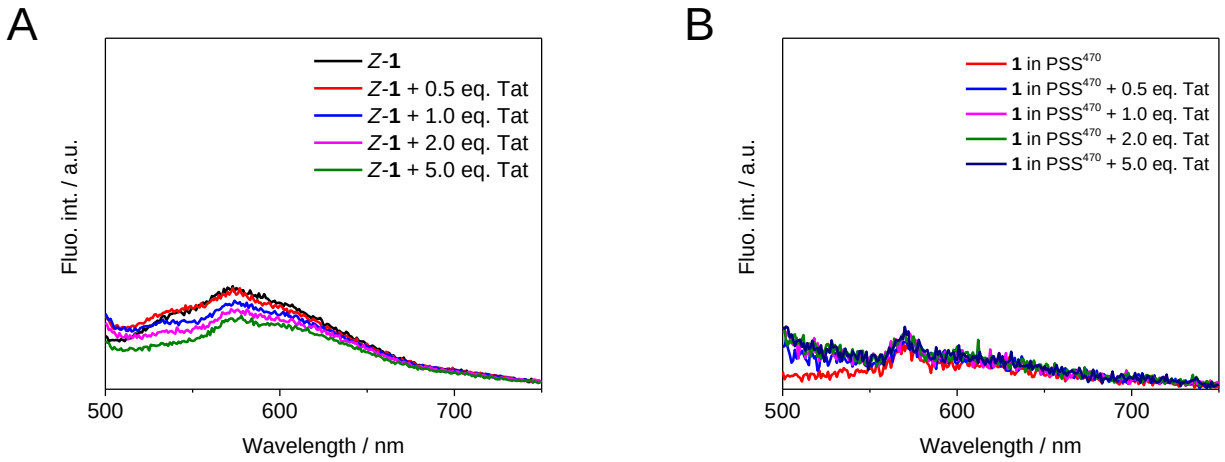


**Figure S4.** Fluorescence spectra of (A) *Z*-**1** and (B) photostationary mixture of *Z*- and *E*-isomers (20/80) in $PSS^{470}$ in the presence of the increasing amounts of Tat peptide, $c_1$ = 10 μM, $\lambda_{ex}$ = 478 nm, 10 mM Na-phosphate buffer with 0.1 M NaCl, pH = 7.0, 20 °C. After addition of every Tat aliquote, the solution was thoroughly mixed and incubated for 10 min.

### *3.3. Photoswitching of complexes 1–TAR, 1–RRE and 1–Tat–TAR*

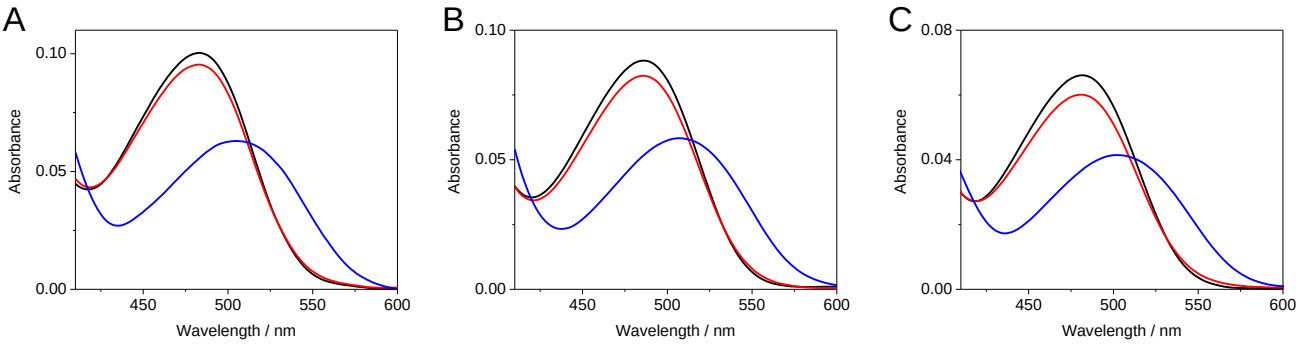


**Figure S5.** Absorption spectra of A: **1**–TAR ($c_1$ = $c_{TAR}$ = 10 μM, $\lambda_{ex}$ = 495 nm), B: **1**–RRE ($c_1$ = $c_{RRE}$ = 10 μM, $\lambda_{ex}$ = 498 nm), C: **1**–Tat–TAR ($c_1$ = $c_{Tat\text{-}TAR}$ = 10 μM, $\lambda_{ex}$ = 480 nm) before irradiation (black), in PSS$^{470}$ (blue) and in PSS$^{590}$ (red); 10 mM Na-phosphate buffer with 0.1 M NaCl, pH = 7.0.

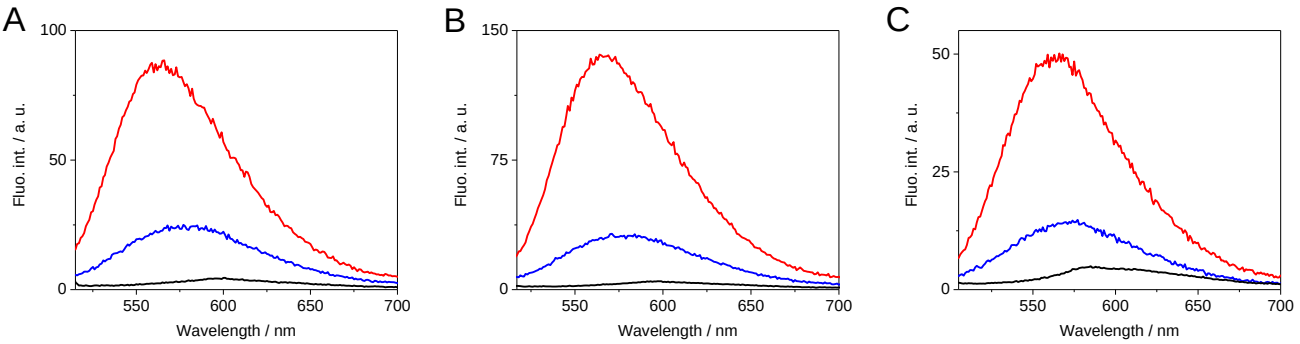


**Figure S6.** Fluorescence spectra of A: **1**–TAR ($c_1$ = $c_{TAR}$ = 10 μM, $\lambda_{ex}$ = 495 nm), B: **1**–RRE ($c_1$ = $c_{RRE}$ = 10 μM, $\lambda_{ex}$ = 498 nm), C: **1**–Tat–TAR ($c_1$ = $c_{Tat\text{-}TAR}$ = 10 μM, $\lambda_{ex}$ = 480 nm) before (red) and after (blue) irradiation with 470 nm LED; corresponding fluorescence spectra of **1** before addition of RNA (black) in each case are black); 10 mM Na-phosphate buffer with 0.1 M NaCl, pH = 7.0.

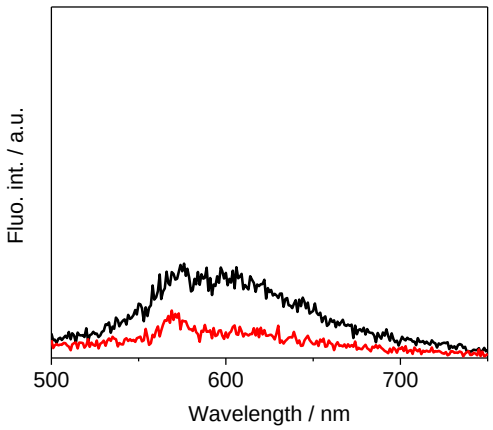


**Figure S7.** Fluorescence spectra of *Z*-**1** (black) and mixture of *Z*- and *E*-isomers (20/80) of **1** in PSS$^{470}$ (red) ($c$ = 10 μM, $\lambda_{ex}$ = 498 nm) in 10 mM Na-phosphate buffer with 0.1 M NaCl, pH 7, 20 °C.

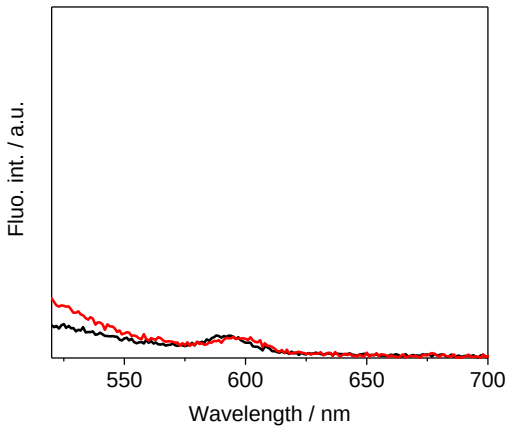


**Figure S8.** Residual fluorescence of TAR RNA (black, $c$ = 10 μM, $\lambda_{ex}$ = 495 nm) and RRE-IIB RNA (red, $c$ = 10 μM, $\lambda_{ex}$ = 498 nm) in 10 mM Na-phosphate buffer with 0.1 M NaCl, pH 7, 20 °C.

Since the excitation wavelengths used for fluorimetric detection of complexes of *Z*-**1** with RNA can induce the isomerization of the ligand, a testing experiment was performed, in which the emission spectra of *Z*-**1**–TAR were measured 15 times in a cyclic mode (Figure S9). Additionally, control absorption spectra of the sample were recorded before and after fluorescence measurements. Both absorption and emission spectroscopy data showed just negligible isomerization of *Z*-**1** upon excitation inside the fluorimeter over 15 records with a scan rate of 120 nm/min. Therefore, switching does not interfere with the conventional detection of fluorescence of *Z*-**1**.

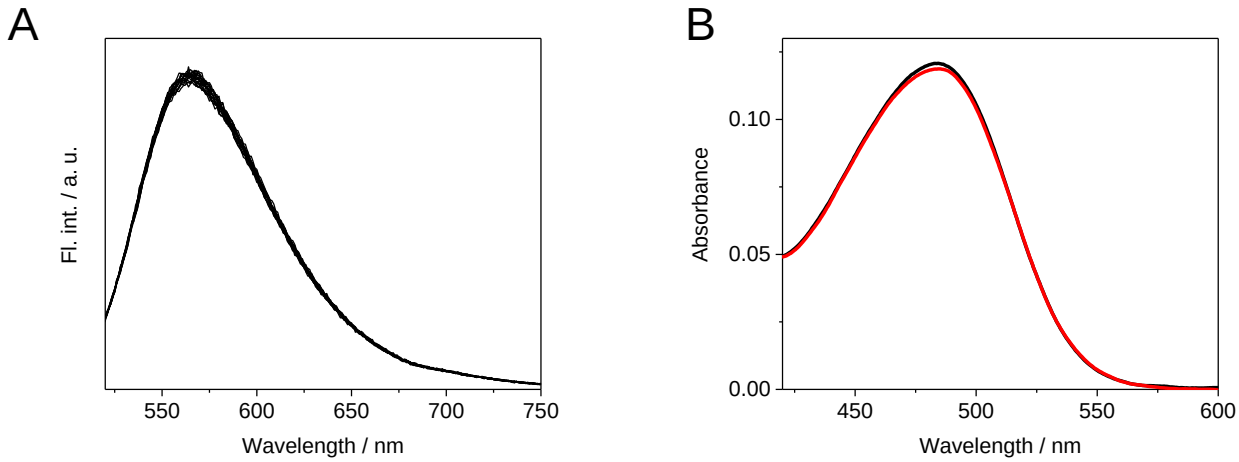


**Figure S9.** (A) Fluorescence spectra of the *Z*-**1**–TAR complex recorded 15 times in a cyclic mode and (B) absorption spectra of *Z*-**1**–TAR sample before (black) and after (red) 15 cycles of fluorescence measurements; $c_{\mathbf{1}} = c_{\mathrm{TAR}} = 10\ \mu\mathrm{M}$, $\lambda_{\mathrm{ex}} = 497$ nm, scan rate 120 nm/min, 10 mM Na-phosphate buffer with 0.1 M NaCl and 1 mM EDTA, pH = 7.0, 20 °C.

### *3.4. Evidence for the interaction of the E-isomer with RNA*

The evidence for the interaction of the photoinduced *E*-isomer of hemi-indigo **1** with TAR and RRE-IIB RNA was obtained upon changing the sequence of irradiation and RNA addition to the solution of *Z*-**1**. For the first sequence, the solution of *Z*-**1** in aqueous buffer was irradiated until $PSS^{470}$ was reached and then 1 eq. of the corresponding RNA was added. For the second sequence, RNA was added to the solution of *Z*-**1** first, and then the obtained mixture was irradiated until $PSS^{470}$ was reached (Figures S10 and S11). For both RNAs, the final spectra ($PSS^{470}$ with 1 eq. of the corresponding RNA) possessed similar shape and the same position of the absorption maxima irrespectively of the way they were obtained.

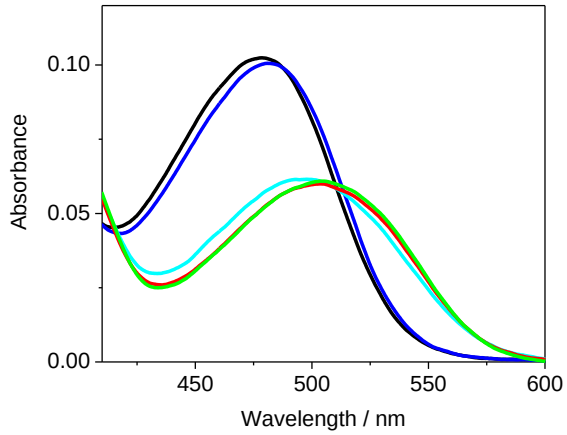


**Figure S10.** Absorption spectra of *Z*-**1** (black), $PSS^{470}$ of **1** (cyan), $PSS^{470}$ of **1** upon addition of 1 eq. of TAR RNA (red); *Z*-**1** with 1 eq. of TAR RNA (blue), $PSS^{470}$ upon irradiation of *Z*-**1** in the presence of 1 eq. of TAR RNA (green). In all cases: $c_1$ = 10 μM, 10 mM Na-phosphate buffer with 0.1 M NaCl , pH = 7, 20 °C.

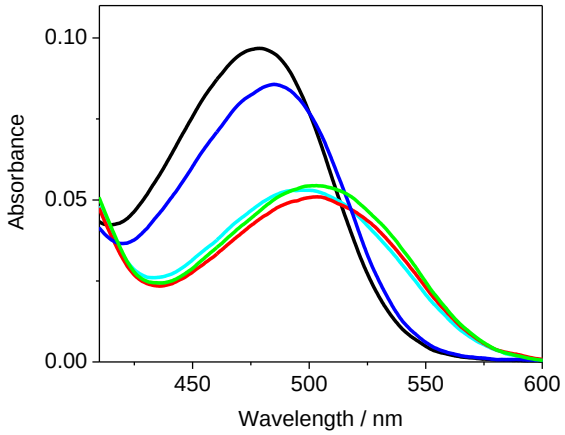


**Figure S11.** Absorption spectra of *Z*-**1** (black), $PSS^{470}$ of **1** (cyan), $PSS^{470}$ of **1** upon addition of 1 eq. of RRE-IIB RNA (red); *Z*-**1** with 1 eq. of RRE-IIB RNA (blue), $PSS^{470}$ upon irradiation of *Z*-**1** in the presence of 1 eq. of RRE-IIB RNA (green). In all cases: $c_1$ = 10 μM, 10 mM Na-phosphate buffer with 0.1 M NaCl , pH = 7, 20 °C.

### *3.5. Estimation of the binding sites of 1*

#### *3.5.1. Displacement studies*

To estimate the binding site of hemi-indigo *Z*-**1**, the displacement experiment with a known TAR RNA binder neomycin[6] was performed (Figure S12). Thus, addition of increasing amounts of neomycin to the solution of *Z*-**1**–TAR complex resulted in gradual quenching of the *Z*-**1** fluorescence that is indicative for the displacement of *Z*-**1** from the TAR RNA. Considering that the binding site for neomycin on TAR is located in the stem immediately below the UCU-bulge,[6] it means that the hemi-indigo ligand also binds in the region of UCU-bulge. Similar experiment was performed with the *E*- and *Z*-isomer mixture of **1** in PSS$^{470}$ (Figure S13).

Although neomycin was also reported in the displacement studies with RRE-IIB RNA,[7] addition of neomycin to *Z*-**1**–RRE complex did not show clear displacement picture. The reason of this can be different binding sites of neomycin and *Z*-**1** on RRE.

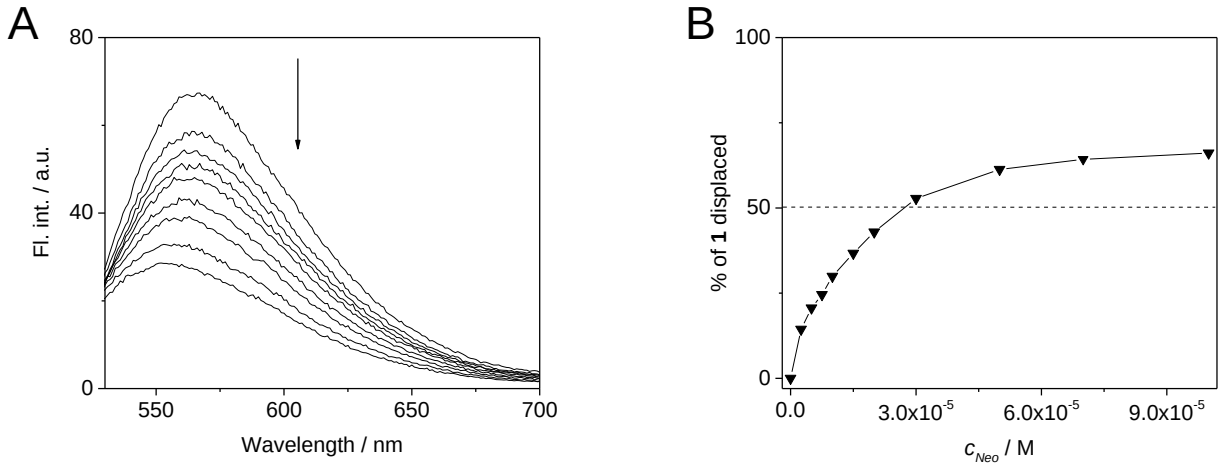


**Figure S12.** (A) Fluorescence quenching upon displacement of *Z*-**1** from TAR RNA by neomycin; (B) the percentage of the displaced ligand **1** *vs* concentration of neomycin; $c_1$ = 10 μM, aliquots of neomycin added (eq.): 0, 0.25, 0.50, 0.75, 1.00, 1.50, 2.00, 3.00, 5.00, 10 mM Na-phosphate buffer with 0.1 M NaCl, pH = 7.0, $\lambda_{ex}$ = 495 nm, 20 °C.

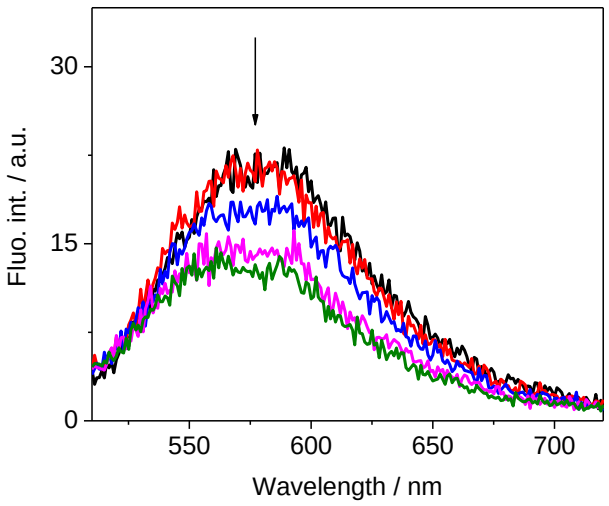


**Figure S13.** Fluorescence quenching upon displacement of **1** in PSS$^{470}$ from TAR RNA by neomycin; aliquots of neomycin added (eq.): 0 (black), 0.5 (red), 1.0 (blue), 2.0 (magenta), 3.0 (green).

### *3.5.2. Circular dichroism spectroscopy studies*

Circular dichroism (CD) spectroscopy is a powerful method to provide an insight into the changes introduced to the secondary structure of RNA by the binding and switching of the ligand. The shape and intensity of the CD bands belonging to the RNA are very sensitive to the spatial rearrangements of the biomolecule. Therefore, CD spectroscopy allows not only to establish the fact of the ligand–RNA interaction but also to estimate the tentative position of the binding site.

The CD spectra of HIV-1 TAR and RRE-IIB RNAs possess three main features: strong positive maxima at 265 nm, weak negative signals at about 240 nm and strong negative minima at 210 nm. Such spectral pattern is characteristic for the A-form of the RNA.[8] The interaction of hemi-indigo *Z*-**1** with TAR RNA produces moderate changes in the TAR structure that is indicated by the decrease in the intensities of the CD bands at 210 nm and 265 nm (Figure S14A). The decrease in the ellipticity at 265 nm is associated with the unstacking of the bases in the UCU-bulge region.[9] Therefore, binding of the hemi-indigo ligand occurs near the bulged region of TAR RNA that is in accordance with the displacement analysis (Figure S12).

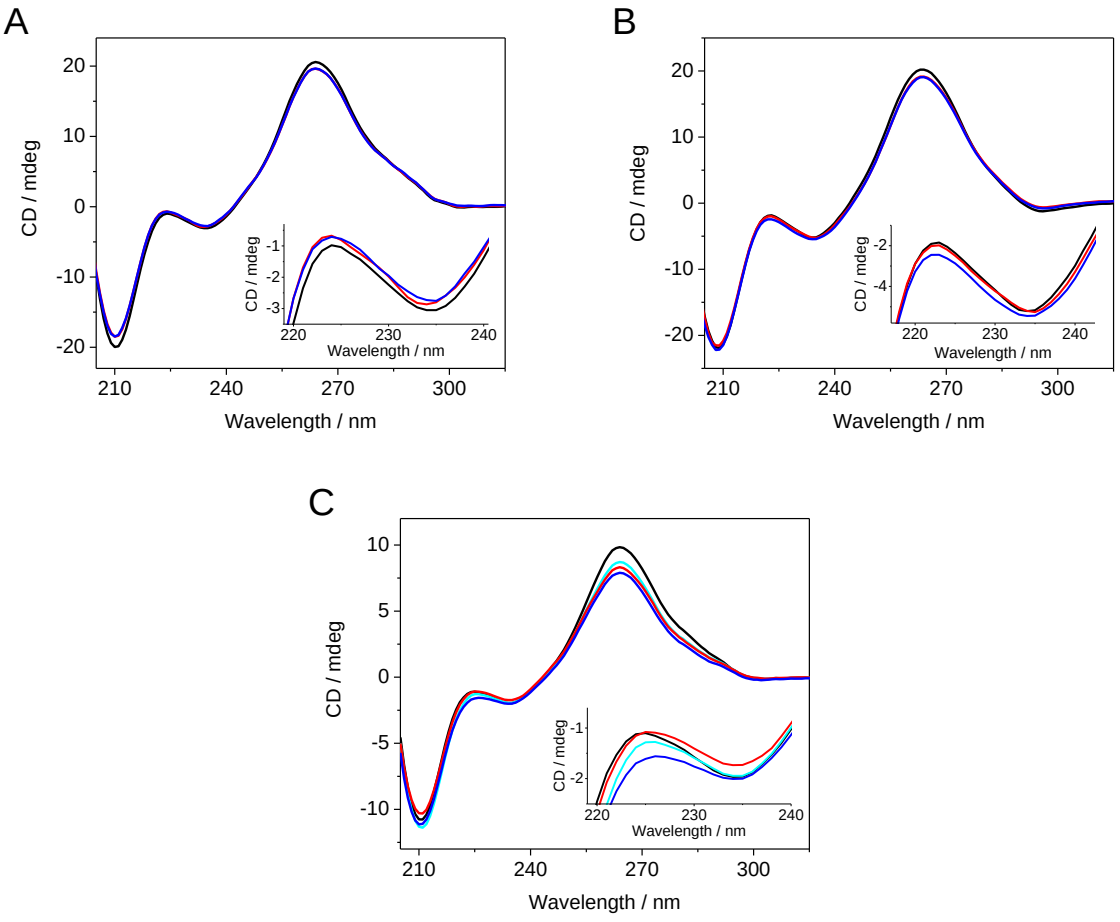


**Figure S14.** CD spectra of (A) TAR RNA (black, $c_{TAR}$ = 2 μM), *Z*-**1**–TAR complex (red, $c_{TAR}$ = 2 μM, $c_{Z\text{-}1}$ = 4 μM), *Z*-**1**–TAR complex irradiated by 470 nm LED (blue), pathlength = 1 cm; (B) RRE-IIB RNA (black, $c_{RRE}$ = 2 μM), *Z*-**1**–RRE complex (red, $c_{RRE}$ = 2 μM, $c_{Z\text{-}1}$ = 10 μM), *Z*-**1**–RRE complex irradiated by 470 nm LED (blue), pathlength = 1 cm; (C) Tat–TAR complex (black, $c_{TAR}$ = $c_{Tat}$ = 5 μM), Tat–TAR–*Z*-**1** complex (red, $c_{TAR}$ = $c_{Tat}$ = 5 μM, $c_{Z\text{-}7}$ = 50 μM), Tat–TAR–*Z*-**1** complex irradiated by 470 nm LED (blue), pathlength = 2 mm. In all cases: 10 mM Na-phosphate buffer with 0.1 M NaCl, pH = 7, 20 °C.

Photoswitching of the TAR-bound ligand to the *E*-form has just a negligible effect on the CD spectrum of the **1**–TAR complex (Figure S14A, inset). This indicates that the photoswitching leads neither to the dissociation of the **1**–TAR complex nor to the change of the binding site of the ligand. Both isomers of **1** remain bound to TAR RNA that is accordance with absorption spectroscopy data (Figure S10). The photoswitching, however, does not induce any rearrangements of the TAR structure.

Like in the case of TAR RNA, association of *Z*-**1** with RRE-IIB RNA leads to the moderate changes in the RRE-IIB structure that is reflected by the decrease of the intensities of the CD bands at 240 nm and 265 nm (Figure 14B). It is difficult, however, to estimate the binding site of *Z*-**1** based on these data. As can be seen from the spectra, upon photoswitching, the hemi-indigo ligand remains bound to RRE-IIB. However, the switching to the *E*-form results in the changes in the spectral region of 220–240 nm (Figure 14B, inset) that may be indicative for the slight ligand-induced structural rearrangement of the RNA. The relatively small extent of the structural changes of both TAR and RRE RNA upon interaction with hemi-indigo **1** can be explained by the small size of the ligand.

The most interesting results were obtained for the binding of hemi-indigo *Z*-**1** to the Tat–TAR complex (Figure 14C). First, the interaction of Tat protein with TAR RNA significantly affects the UCU-bulge and adjacent base pairs of the upper steam that is reflected by the changes in the CD spectrum of TAR, especially pronounced for the positive band at 265 nm (Figure 14C).[10] Association of *Z*-**1** with the Tat–TAR complex results in further decrease of the CD band at 265 nm indicating further unstacking of the bases in the UCU-bulge region. Considering the fact that Tat protein binds at the bulge region from the major groove side,[11,12] it can be assumed that hemi-indigo *Z*-**1** binds near the bulge from the minor groove side. Interestingly, the sequence of mixing the components does not affect the final spectrum of the ternary **1**–Tat–TAR complex. Most notably, the **1**–Tat–TAR complex is stable, although in general formation of such systems is not favored. For example, formation of the ternary complex between TAR RNA, Tat protein and neomycin induces dissociation of Tat from the complex by allosteric mechanism.[6] Moreover, no displacement of the Tat protein is observed even at the excess of the ligand. Photoswitching of the hemi-indigo within the ternary complex is still efficient and produces more pronounced structural changes in RNA in comparison to the binary ligand–RNA complexes (Figure 14C). The CD spectrum obtained after irradiation of **1**–Tat–TAR indicates that all the components remain bound in the ternary species. Noticeable structural rearrangement upon switching of **1** to the *E*-form can be explained by additional stiffening of the RNA upon binding of Tat that makes the binding site of the ligand more spatially restricted. Overall, these results point out that hemi-indigo scaffold can be perspective for the light-induced structural manipulation of RNA upon introduction of appropriate bulky substituents that will increase the spatial influence of the ligand.

### *3.6. Calculation of the extent of the Z-E conversion by Fischer method*

Since the solubility of hemi-indigo **1** in water was not good enough to determine the isomeric compositions of PSS by NMR spectroscopy, the Fischer method was applied to determine the extent of the *Z*-*E* conversion $\alpha$ upon irradiation with 470 nm LED and to calculate the absorption spectra of pure *E*-isomers of hemi-indigo derivatives.[3] The Fischer method can be applied to reversible photochemical systems comprising only two interconverting components A ↔ B (starting form and photoinduced form) that are stable both thermally and photochemically to make possible the establishment of true photostationary states. Thus, for every case the absorption spectrum of the starting *Z*-isomer of hemi-indigo and the absorption spectra of two photostationary states obtained by irradiation of the solutions of the *Z*-isomer at two different wavelengths (470 nm and 520 nm) were recorded (Figure S15). Assuming that the ratio of the quantum yields of the backward and forward reactions ($\varphi_{Z\rightarrow E}/\varphi_{E\rightarrow Z}$) is independent of the irradiation wavelength, the fraction of the *Z*-isomer in each photostationary state, the absorption spectrum of the *Z*-isomer (Figure S15) and the extent of the *Z*-*E* conversion $\alpha$ (Table S1) were calculated. It was independently established that both *E*- and *Z*-forms of hemi-indigo **1** remain completely bound to RNA under saturation conditions resulting in a quasi A ↔ B system. Therefore, application of the Fischer method for the photoswitching of hemi-indigo **1** in the presence of the studied biomolecules is justified. Since the interaction of **1** with Tat–TAR complex does not reach the saturation of binding, the calculations for this system cannot be performed.

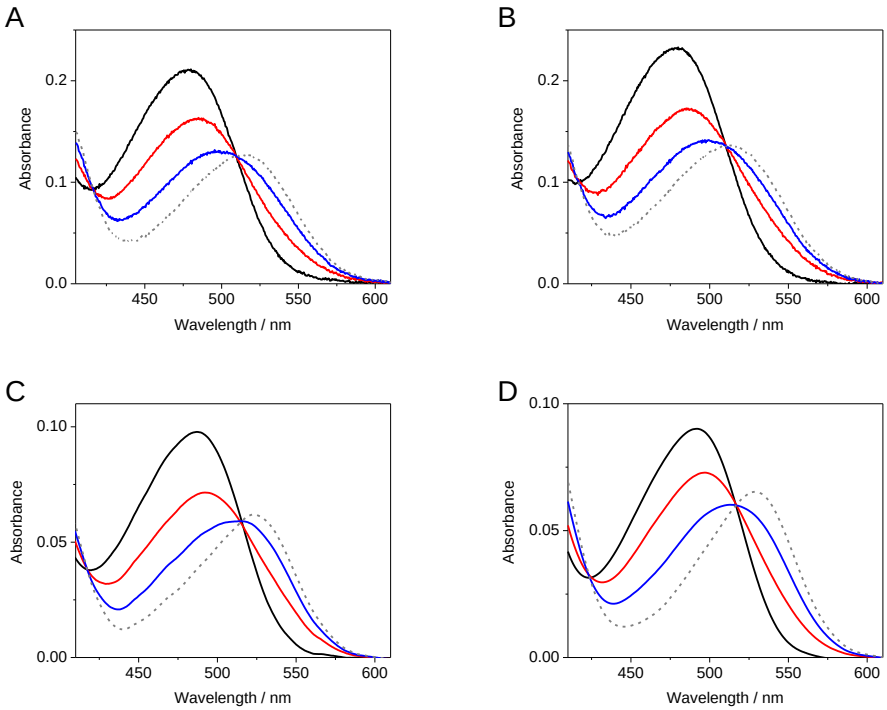


**Figure S15.** Absorption spectra of *Z*-**1** (black) and two photostationary states obtained upon irradiation with 520 nm (red) and 470 nm (blue) light; grey dashed line represents the spectrum of *E*-**1** form calculated by Fischer method. A: free **1** in deionized water ($c$ = 20 μM); B: free **1** in 10 mM Na-phosphate buffer with 0.1 M NaCl, pH = 7.0 ($c$ = 20 μM); C: **1** bound to TAR RNA ($c_1$ = 7 μM, $c_{TAR}$ = 28 μM); D: **1** bound to RRE IIB RNA ($c_1$ = 1 μM, $c_{RRE}$ = 28 μM). In the case of graphs C and D: 10 mM Na-phosphate buffer with 0.1 M NaCl, pH = 7.0, both *E*- and Z-isomers of **1** remain bound to the corresponding biomolecules.

Based on the calculated absorption spectra of the *E*-isomer and the experimental absorption spectra of obtained for free **1** and its complexes **1**–TAR and **1**–RRE (Figure S5; Figure 1, main text), the extents of *Z*-*E* conversion for $PSS^{590}$ were calculated by Fisher method, as described above. The obtained values are collected in Table S1.

**Table S1.** Extents of *Z*-*E* conversion $\alpha$ of hemi-indigo **1** in $PSS^{470}$ and $PSS^{590}$ under different conditions calculated by Fischer method ($\alpha$ corresponds to the percentage of the photoinduced *E*-form).

| | **1** (water) | **1** (buffer) | **1**–TAR | **1**–RRE IIB |
|---|---|---|---|---|
| $\alpha^{470}$ | 0.76 | 0.80 | 0.77 | 0.71 |
| $\alpha^{590}$ | 0.03 | 0.03 | 0.08 | 0.11 |

**Table S2.** Absorption maxima and corresponding molar extinction coefficients for *Z*- and *E*-isomers of hemi-indigo **1** and its complexes with RNA.

| Species | $\lambda_{abs}$ (*Z*) / nm | $\lambda_{abs}$ (*E*) / nm [a] | $\varepsilon$(*Z*) / L mol$^{-1}$ cm$^{-1}$ | $\varepsilon$(*E*) / L mol$^{-1}$ cm$^{-1}$ [a] |
|---|---|---|---|---|
| **1** | 478 | 514 | 10456 | 6289 |
| **1**–TAR | 488 | 523 | 9084 | 5839 |
| **1**–RRE | 493 | 529 | 8696 | 6365 |

[a] calculated by Fisher method

### *3.7. Calculation of the photoisomerization quantum yields*

The quantum yield of *Z*-*E* isomerization was determined upon irradiation with 470 nm (blue) light. The quantum yield of *E*-*Z* isomerization was determined upon irradiation with 590 nm (amber) light. In the used setup, the irradiation was performed by placing a LED on the top of a photometric cell. The LED output went through the round aperture with a diameter of 3 mm. Reinecke salt $NH_4[Cr(NCS)_4(NH_3)_2]\times H_2O$ was used as a chemical actinometer for the determination of the intensity of the visible light source.[4] A concentrated solution of Reinecke salt in water was prepared, filtered to remove undissolved residue and acidified to pH = 5.3–5.5 by addition of a calculated amount of 0.01 M $H_2SO_4$. Samples of the prepared solution of the actinometer ($V_{samp}$ = 0.35–0.40 mL) were irradiated for different time intervals; then the aliquots ($V_{aliq}$ = 0.05 mL) of the irradiated samples were taken and diluted with 6.2 mL of 0.1 M solution of $Fe(NO_3)_3$ in 0.5 M $HClO_4$ to the final volume ($V_{dil}$ = 6.25 mL). The absorbance of the obtained mixtures was determined photometrically at the absorption maximum of iron (III) rhodanide ($\lambda_{max}$ = 450 nm). The obtained absorbance values were plotted *vs* irradiation time and fitted to a linear dependence. The first derivative of the linear fit gave the *D*/*t* ratio.

The light intensity was calculated as following:

$$I_0 = 0.001 \cdot \frac{V_{dil}}{V_{aliq}\,\varepsilon\, l} \cdot \frac{1}{\Phi} \cdot \frac{D}{t} \cdot \frac{1}{(1 - 10^{-\varepsilon' c' l})} \qquad \text{(Eq. 1)}$$

where $I_0$ is the intensity of the light source (einstein $L^{-1}$ $s^{-1}$), $\Phi$ is the quantum yield of the rhodanide-anions formation at irradiation wavelength, $\varepsilon$ is the extinction coefficient of the iron (III) rhodanide at 450 nm ($\varepsilon$ = 4300 $M^{-1}$ $cm^{-1}$), $l$ is the irradiation path (cm).

The correction coefficient ($1 - 10^{-\varepsilon' c' l}$) was introduced to compensate the residual transmittance of the actinometer solution at the irradiation wavelength; $\varepsilon'$ is the extinction of the Reinecke salt at irradiation wavelength ($\varepsilon'_{470}$ = 50.0 $M^{-1}$ $cm^{-1}$, $\varepsilon'_{590}$ = 38.9 $M^{-1}$ $cm^{-1}$), $c'$ is the actual concentration of the actinometer solution determined photometrically before the measurement (for irradiation experiment at 470 nm: $c'$ = 0.0212 M; for irradiation experiment at 590 nm: $c'$ = 0.0225 M). The obtained values of the light intensity are $I_0^{470}$ = 3.841E-08 einstein $L^{-1}$ $s^{-1}$ for 470 nm LED and $I_0^{590}$ = 1.088E-08 einstein $L^{-1}$ $s^{-1}$ for 590 nm LED.

Photoisomerization quantum yields were calculated according to Eq. 2.

$$\Phi = \frac{\Delta A/\Delta t}{I_0\left(1 - 10^{-A'}\right) \cdot \varepsilon \cdot 1000} \qquad \text{(Eq. 2)}$$

where $\Delta A/\Delta t$ is the change of absorbance at the detection wavelength within the time, $I_0$ is the intensity of the light source, A′ is the initial absorption of the sample at the irradiation wavelength, $\varepsilon$ is the extinction coefficient at the detection wavelength.

For the forward *Z*-*E* switching of **1**, **1**–TAR and **1**–RRE that starts from 100% of the *Z*-isomer, $\Delta A/\Delta t$ corresponds to the initial slope of the *A vs t* kinetics recorded at the wavelength, where the absorbance of the *Z*-isomer is close to zero ($\lambda_{det}$ = 565 nm for **1** and **1**–TAR; $\lambda_{det}$ = 575 nm **1**–RRE). For the backward *E*-*Z* switching the initial solutions were pre-irradiated at 470 nm, therefore, the backward reaction started form the corresponding mixtures of *E*- and *Z*-isomers. To apply the initial slope method in this case, the *A vs t* kinetics was fitted to a polynomial dependence and extrapolated to the zero absorbance of the *Z*-isomer (Figure S16).[5] The initial slope was obtained by the insertion of the extrapolated *t* value to the 1st derivative of the fitting polynomial.

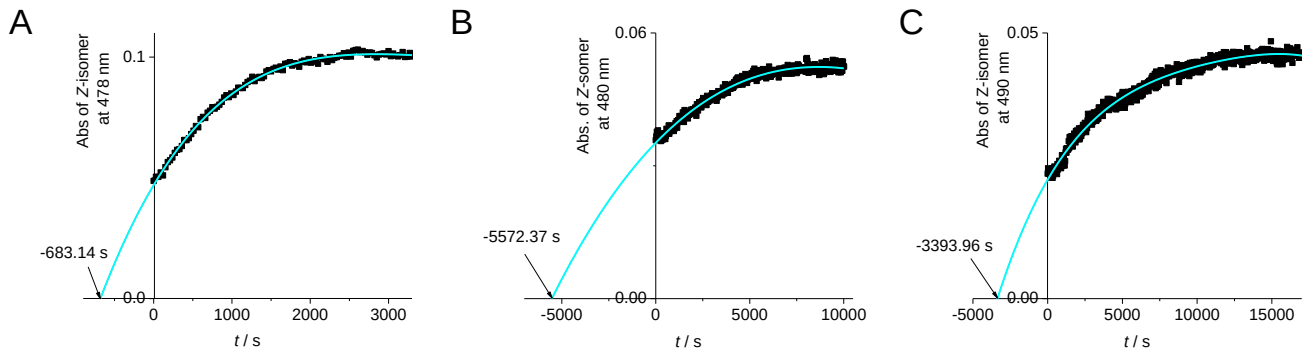


| | | |
|---|---|---|
| $y = 0.047 + 5.441\text{E-}5x -$ $- 1.942\text{E-}8x^2 + 2.917\text{E-}12x^3 -$ $- 1.597\text{E-}16x^4$ | $y = 0.035 + 4.381\text{E-}6x -$ $-3.266\text{E-}10x^2 + 5.663\text{E-}15x^3$ | $y = 0.022 + 4.836\text{E-}6x -$ $- 4.562\text{E-}10x^2 + 2.390\text{E-}14x^3 -$ $- 5.318\text{E-}19x^4$ |
| $y' = 5.441\text{E-}5 - 3.887\text{E-}8x +$ $+ 8.752\text{E-}12x^2 - 6.387\text{E-}16x^3$ | $y' = 4.381\text{E-}6 - 6.532\text{E-}10x +$ $+ 16.990\text{E-}15x^2$ | $y' = 4.836\text{E-}6 - 9.125\text{E-}10x +$ $+ 7.169\text{E-}14x^2 - 21.274\text{E-}19x^3$ |

**Figure S16.** Quantum yield measurement of the *E*-*Z* photoisomerization of hemi-indigo **1** (A) and complexes **1**–TAR (B) and **1**–RRE (C) upon irradiation with 590 nm LED starting from the pre-irradited mixtures of *E*- and *Z*-isomers (black squares), 10 mM Na-phosphate buffer with 0.1 M NaCl, pH = 7.0. The whole photoconversion kinetics was fitted to the corresponding polynomials (cyan solid line).

### *3.8. Calculation of the E-isomer half-lives*

Thermal dark *E*-*Z* relaxation kinetics of hemi-indigo **1** and its complexes with TAR and RRE-IIB RNA were followed by UV-Vis spectroscopy at 40 °C. It was considered that at this temperature no significant perturbation of the RNA secondary structure occurs (TAR RNA sequence melts at 72 °C and RRE-IIB RNA sequence melts at 82 °C, according to the supplier's specification). Thermal *E*-*Z* relaxation of the ternary system **1**–Tat–TAR were not measured due to denaturation of Tat protein upon heating.

Considering that the thermal *E*-*Z* isomerization for hemi-indigo **1** is a unimolecular first order reaction that proceeds completely to the pure *Z*-isomer, Eq. 3 can be applied:[5]

$$-\frac{d[E]}{dt} = \frac{d[Z]}{dt} = k[E] \qquad \text{(Eq. 3)}$$

where *k* is the rate constant of the thermal *E*-*Z* relaxation at a certain temperature.

The rate constants *k* were obtained from the exponential fitting of the thermal dark *E*-*Z* relaxation of the pre-irradiated by 470 nm light photostationary mixture of *E*- and *Z*-isomers of **1** monitored at 40 °C. In the case of free **1**, the kinetics was fitted to a monoexponential dependence that gave the *k* value directly (Figure S17A). In the case of the complex **1**–RRE, the kinetics was fitted to a biexponential dependence, most likely, due to the presence of the minor amount of the second ligand–RNA complex of different stoichiometry at 40 °C (Figure S17B). However, the analysis of the fit revealed that the contribution of the second exponential component to the kinetics is just 2.91%. Therefore, it was neglected, and the rate constant for the complex **1**–RRE was calculated considering the main (97.09%) exponential component. In the case of the complex **1**–TAR, the reliable dark relaxation kinetics could not be obtained. Possible reason of this can be binding of hemi-indigo **1** to different binding sites of TAR RNA, as expected from the photometric titration data (Figure 3, main text).

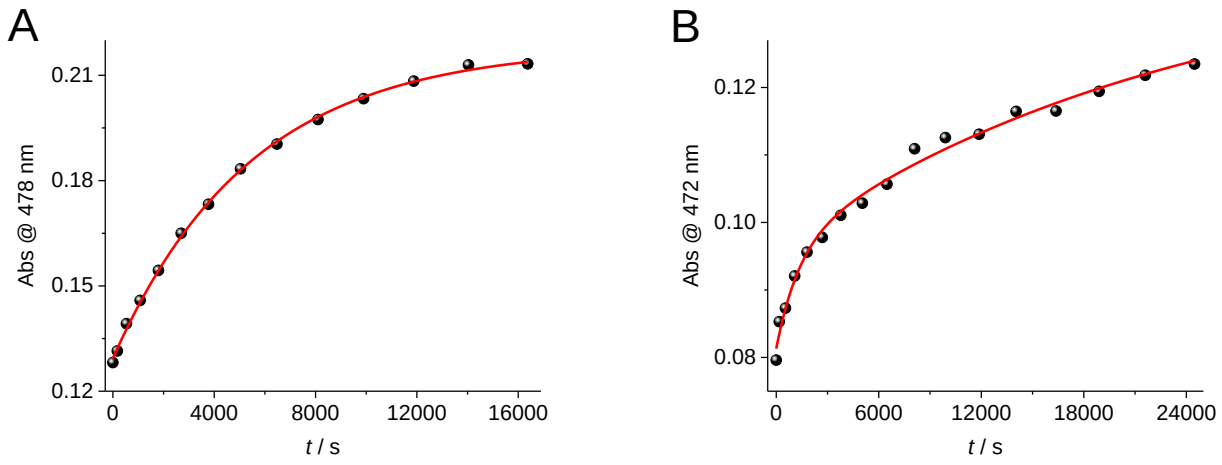


$k = (1.84 \pm 0.06) \times 10^{-4}$ s$^{-1}$
$\chi^2 = 8.88787\text{E-}7$
$r^2 = 0.99907$

$k_1 = (7.51 \pm 1.88) \times 10^{-4}$ s$^{-1}$ (2.91%)
$k_2 = (4.19 \pm 0.30) \times 10^{-5}$ s$^{-1}$ (97.09%)
$\chi^2 = 1.61857\text{E-}6$
$r^2 = 0.99115$

**Figure S17.** Evolution of the absorbance (black spheres) for the thermal *E*-*Z* isomerization in 10 mM Na-phosphate buffer with 0.1 M NaCl, pH = 7.0, at 40 °C of (A) **1**, $\lambda_{det}$ = 478 nm; (B) **1**–RRE, $\lambda_{det}$ = 472 nm; solid red line indicates the fit of the experimental data to the mono- or biexponential model.

*Eyring* equation was used for the calculation of the free activation enthalpy Δ*G** of the *E*-*Z* isomerization:[5]

$$k = \frac{k_B T}{h} e^{-\frac{\Delta G^*}{RT}} \qquad \text{(Eq. 4)}$$

where $k_B$ is Boltzmann constant, *h* is Plank constant, *R* is the universal gas constant, *T* is temperature in K. Considering the numerical values of the constants, Eq. 4 can be rearranged as following:

$$\Delta G^* = 8.314T \cdot \left(23.760 + \ln\left(\frac{T}{k}\right)\right) \qquad \text{(Eq. 5)}$$

Using the obtained Δ*G** values, the half-lives of the *E*-isomer of **1** at 25 °C were calculated (Table S3, Table 1 in the main text).

**Table S3.** Free activation enthalpies Δ*G** for the thermal *E*-*Z* isomerization and corresponding half-lives at 25 °C of hemi-indigo **1** in free and RNA-bound state.

| Species | Δ*G** (*E*-*Z*)/ kcal mol$^{-1}$ | $\tau$ / h |
|---|---|---|
| **1** | 23.7 | 10.8 |
| **1**–RRE | 24.6 | 51.0 |

### *3.9. Calculation of the binding constants for 1–RNA complexes*

The binding constants of the complexes of hemi-indigo *Z*-**1** with TAR and RRE-IIB RNA were determined using SpecFit/32 [Spectrum Software Associates, PMB 361, 197M Boston Post Road, West Marlborough, MA 01752, U.S.A.] from the binding isotherms obtained from the fluorimetric titrations data (Figure S18). Due to the small size of the used RNA oligonucleotides (TAR – 29 bases, RRE-IIB – 34 bases) and their well-defined secondary structure and tertiary folding, the ligand–oligonucleotide binding can be represented as a host–guest interaction, where one host molecule (RNA) provides one or several binding sites for the guest molecules (*Z*-**1**). For both TAR and RRE-IIB RNA, the following equilibria were considered to occur simultaneously or separately:

Lig + RNA ⇔ Lig-RNA

2Lig + RNA ⇔ $(Lig)_2$-RNA

3Lig + RNA ⇔ $(Lig)_3$-RNA

However, in both cases the best fit of the theoretical model to the experimental data was reached if exclusively 1:1 stoichiometry was considered, whereas consideration of 2:1 and 3:1 (Lig-RNA) stoichiometries led to the divergence of the fit.

Therefore, 1:1 stoichiometry was taken as preferred for both TAR and RRE-IIB oligonucleotides and the further calculation was performed for this binding model, yielding the binding constant values of $K$ = 1.1 x $10^5$ $M^{-1}$ for *Z*-**1**–TAR and $K$ = 1.7 x $10^5$ $M^{-1}$ for *Z*-**1**–RRE.

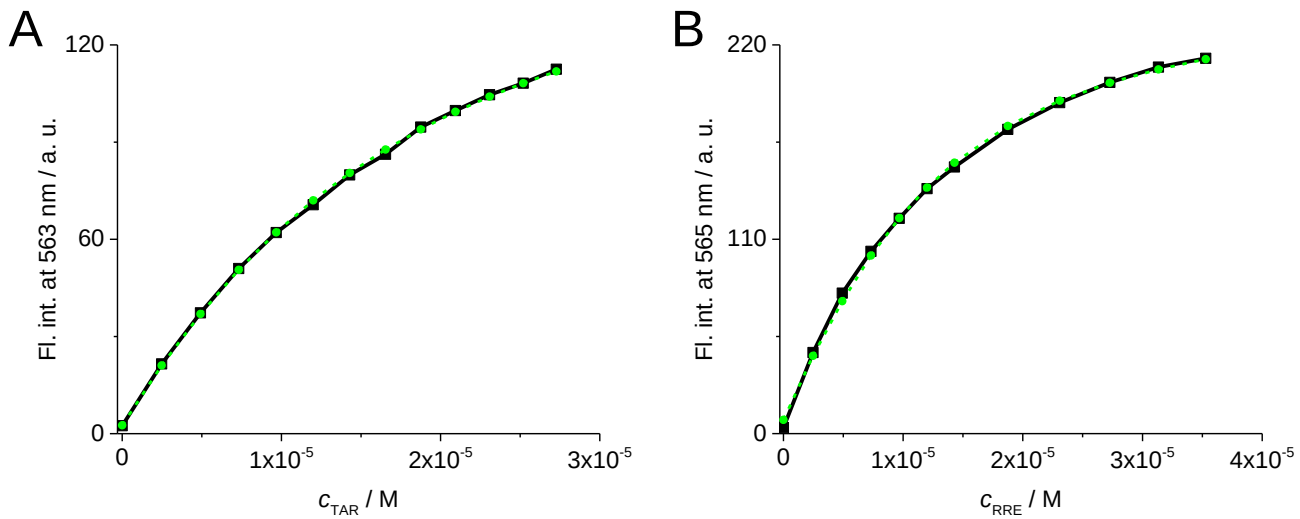


**Figure S18.** Binding isotherms, i.e. plots of fluorescence intensity of *Z*-**1** versus $c_{RNA}$, obtained from the fluorimetric titrations of *Z*-**1** with (A) TAR RNA and (B) RRE-IIB RNA; black solid line: experimental data, green dashed line: fit to the theoretical model.

## 4. NMR data

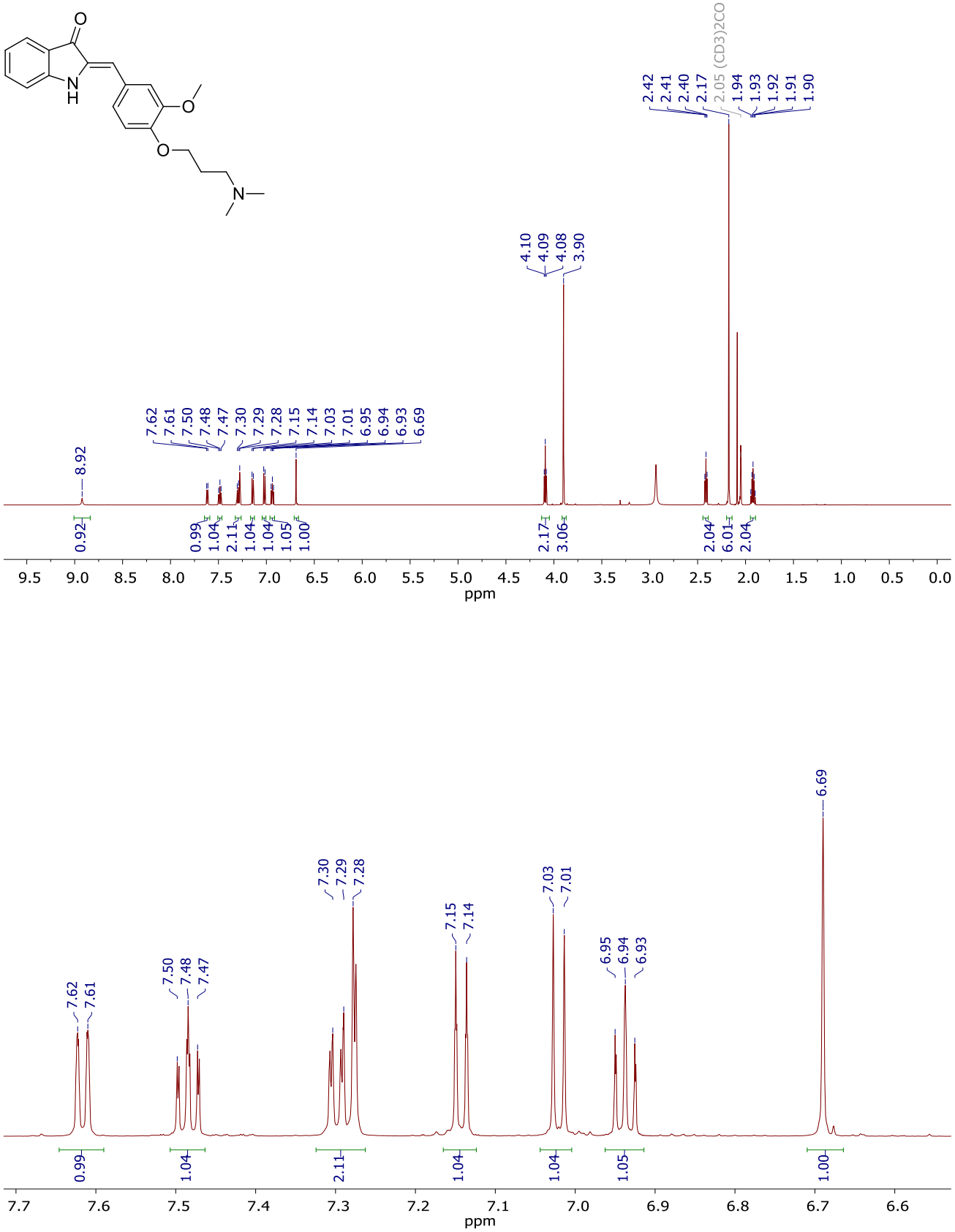


**Figure S19.** $^{1}$H NMR spectrum of *Z*-**1** in acetone-$d_6$ (top) with an expansion of the aromatic proton signals region (bottom).

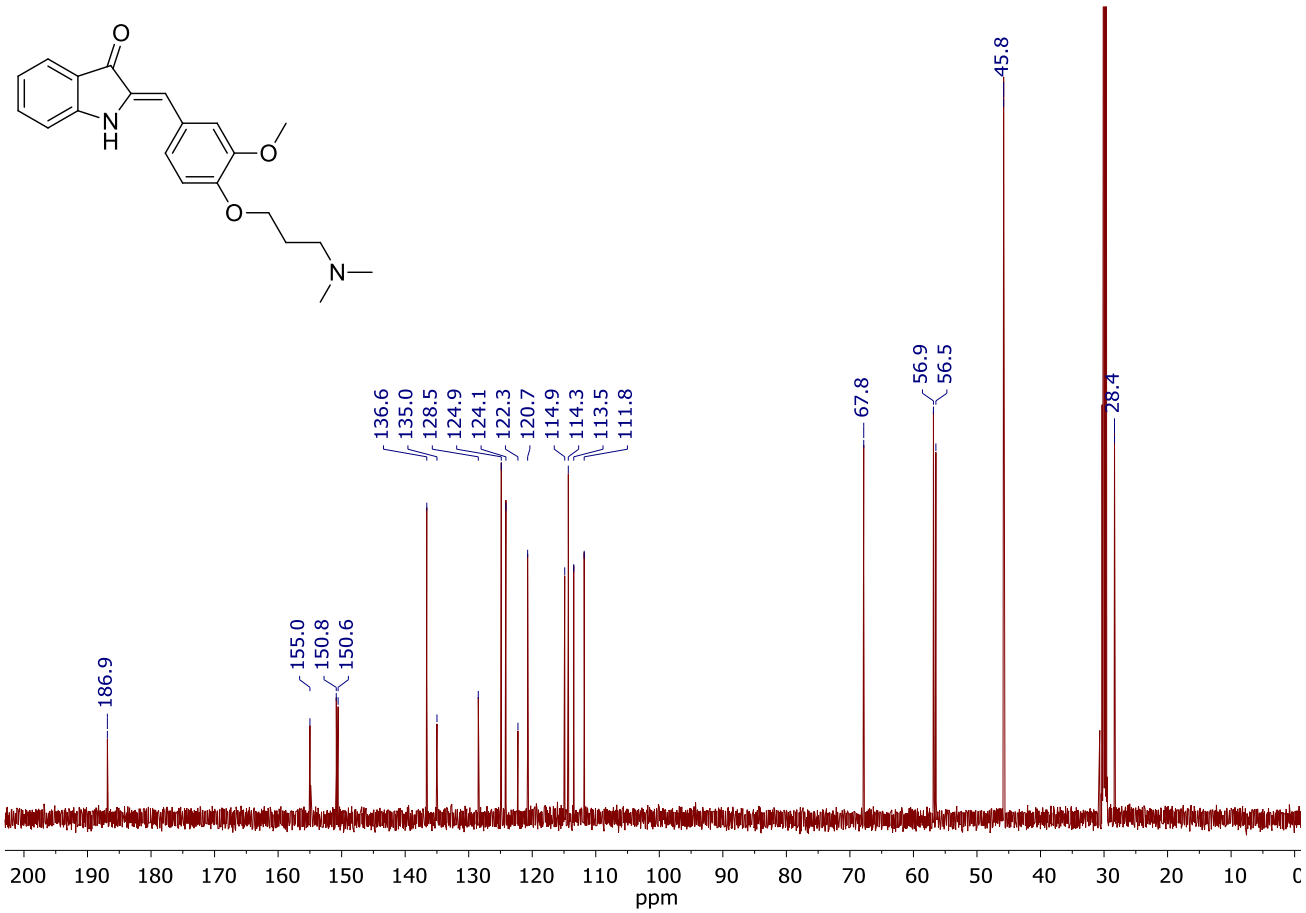


**Figure S20.** $^{13}$C NMR spectrum of *Z*-**1** in acetone-$d_6$.

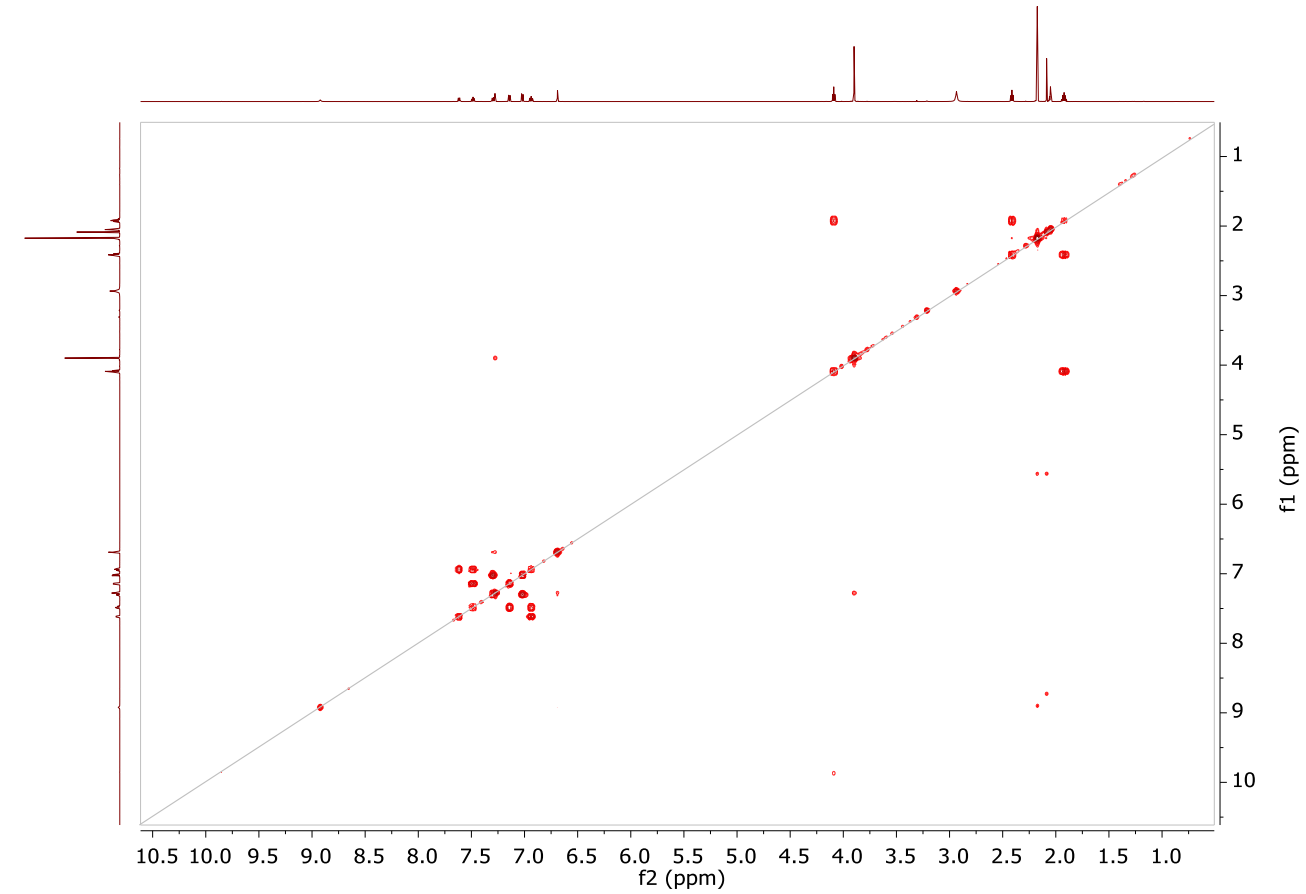


**Figure S21.** {$^1$H, $^1$H}-COSY NMR spectrum of *Z*-**1** in acetone-$d_6$.

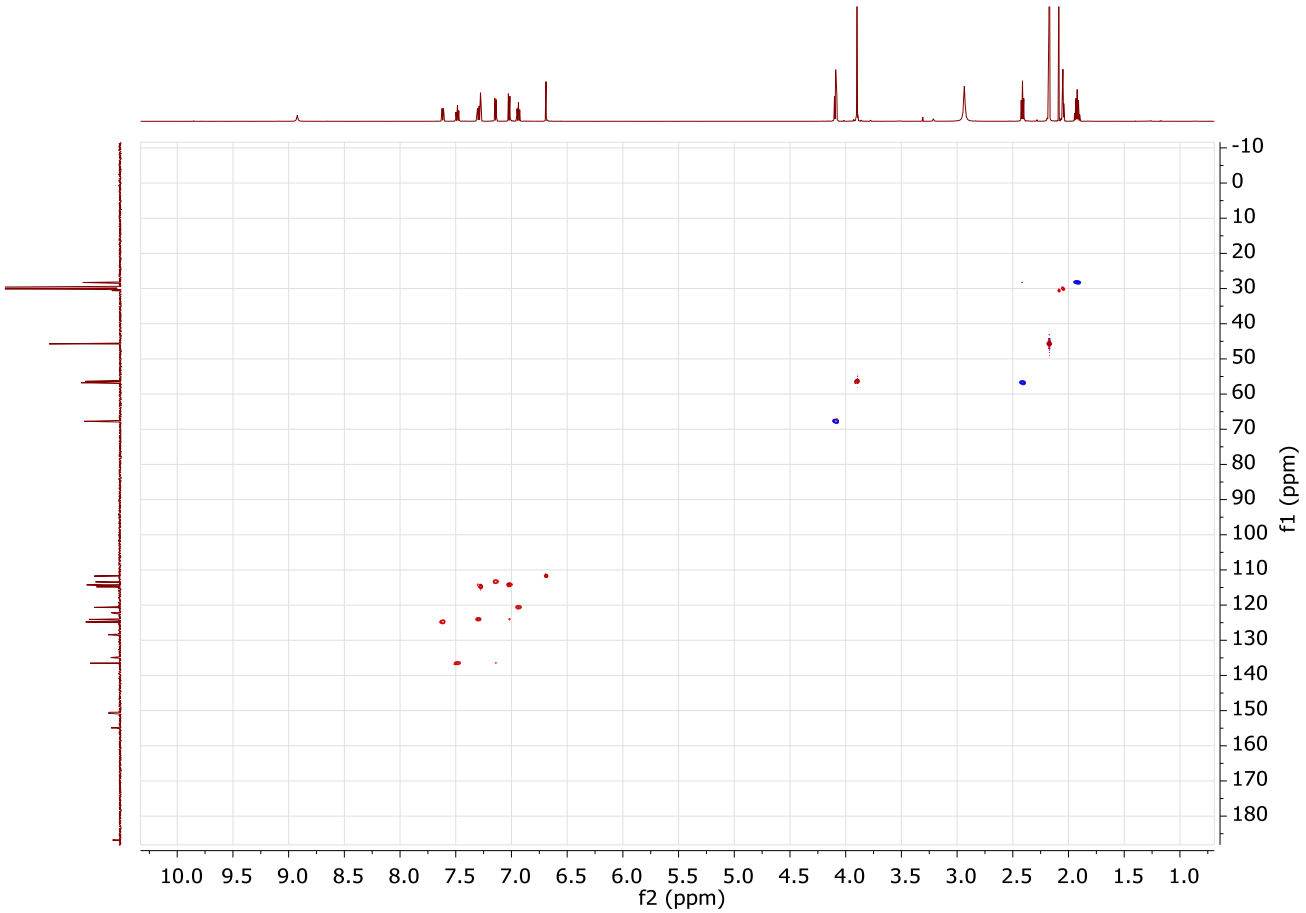


**Figure S22.** HMQC NMR spectrum of *Z*-**1** in acetone-$d_6$.

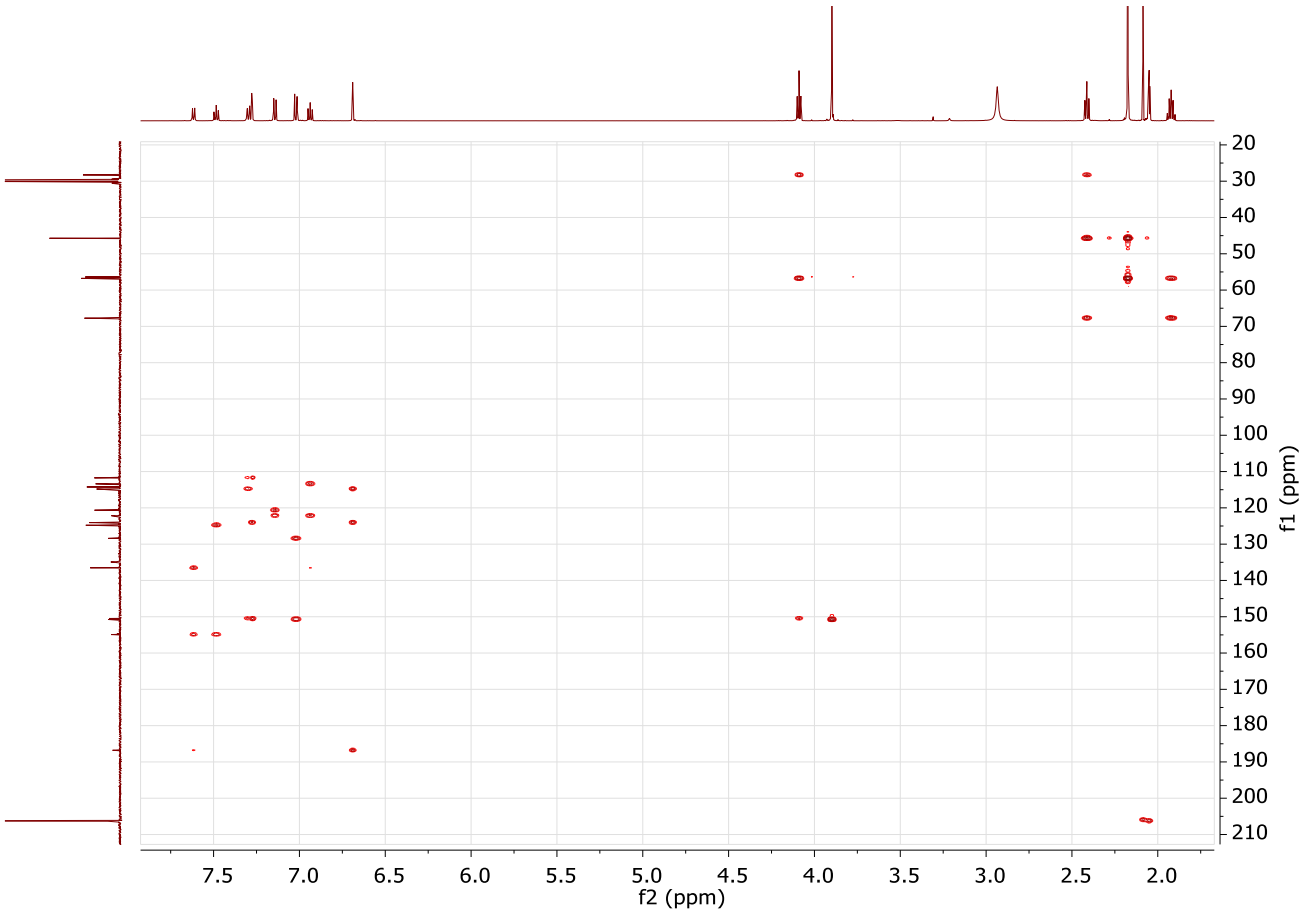


**Figure S23.** HMBC NMR spectrum of *Z*-**1** in acetone-$d_6$.

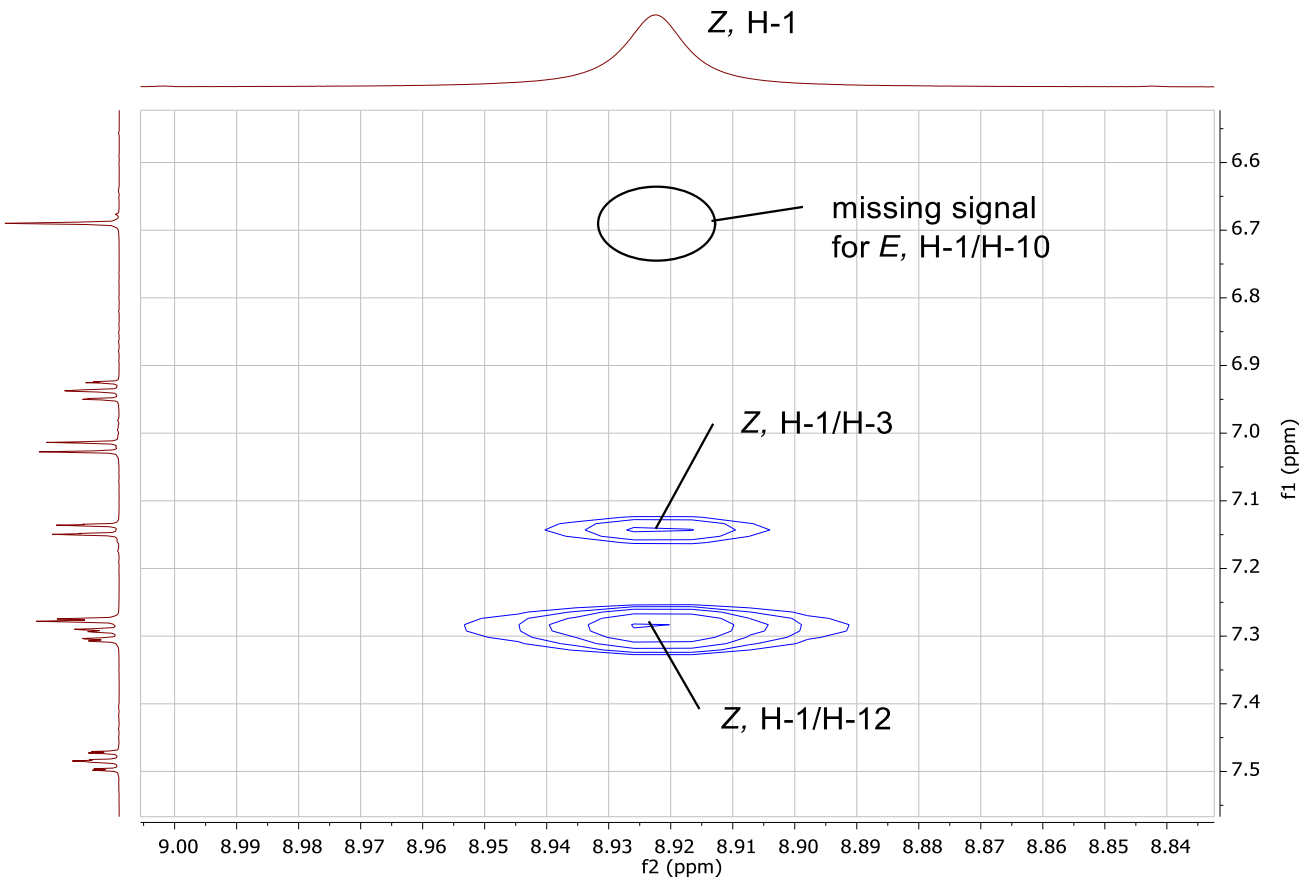


**Figure S24.** Section of the ROESY NMR spectrum of hemi-indigo *Z*-**1** in acetone-$d_6$. The ROE cross signal between protons H-1 and H-12 indicate their close proximity and, therefore, prove the *Z*-conformation. In the *E*-conformation a cross signal between protons H-1 and H-10 is expected but it is not observed.

## 5. Characteristics of LEDs

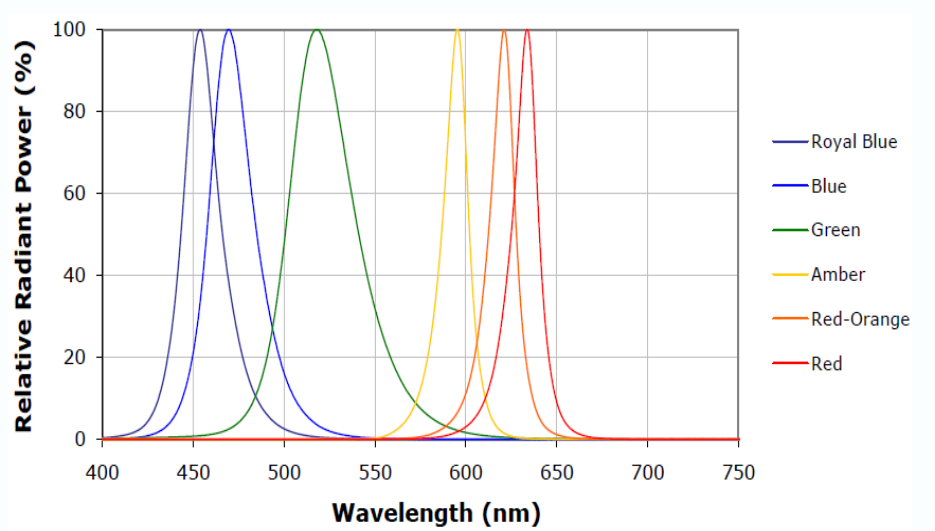


**Figure S25.** Emission of the visible-range LEDs (spectra are taken from the producer's specification). In this study, blue (470 nm), green (520 nm) and amber (590 nm) LEDs were used.

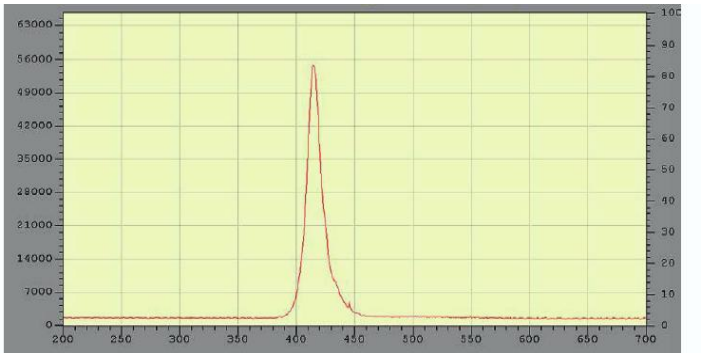

**Figure S26.** Emission of the blue LED (420 nm) (spectrum is taken from the producer's specification).

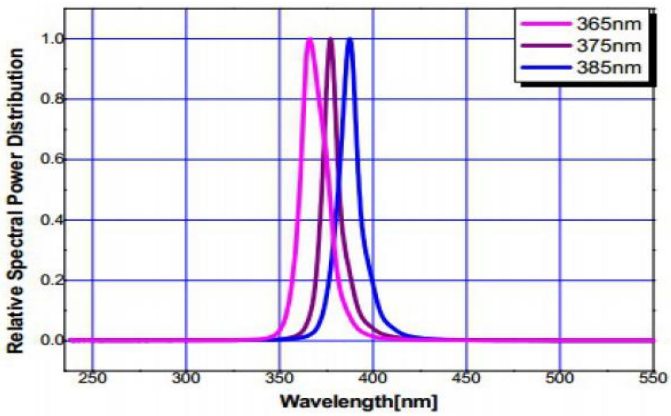


**Figure S27.** Emission of the UV LEDs (spectra are taken from the producer's specification). In this study, a 365 nm LED was used.

## 6. References

(1) N. Malecki, P. Carato, B. Rigo, J.-F. Goossens, R. Houssin, C. Bailly, J.-P. Hénichart, *Bioorg. Med. Chem*. **2004**, *12*, 641.

(2) C. Dingwall, I. Ernberg, M. J. Gait, S. M. Green, S. Heaphy, J. Karn, A. D. Lowe, M. Singh, M. A. Skinner, *EMBO Journal* **1990**, *9(12)*, 4145.

(3) E. Fischer, *J. Phys. Chem*. **1967**, *71*, 3704.

(4) E. W. Wegner, A.W. Adamson, *J. Am. Chem. Soc*. **1966**, *88 (3)*, 394.

(5) C. Petermayer, S. Thumser, F. Kink, P. Mayer, H. Dube, *J. Am. Chem. Soc*. **2017**, *139 (42)*, 15060.

(6) S. Wang, P. W. Huber, M. Cui, A. W. Czarnik, H.-Y. Mei, *Biochemistry* **1998**, *37(16)*, 5549–5557.

(7) J. Zhang, S. Umemoto, K. Nakatani, *J. Am. Chem. Soc*. **2010**, *132 (11)*, 3660–3661.

(8) J. H. Riazance, W. A. Baase, W. C. Johnson, K. Hall, P. Cruz, I. Tinoco, *Nucleic Acids Res*. **1985**, *13*, 4983–4989.

(9) S. Wang, P. W. Huber, M. Cui, A. W. Czarnik, H.-Y. Mei, *Biochemistry* **1998**, *37*, 5549–5557.

(10) H. Suryawanshi, H. Sabharwal, S. Maiti, *J. Phys. Chem. B* **2010**, *114 (34)*, 11155–11163.

(11) J. D. Puglisi, R. Tan, B. J. Calnan, A. D. Frankel, J. R. Williamson, *Science* **1992**, *257*, 76–80.

(12) F. Aboul-ela, J. Karn, G. Varani, *J. Mol. Biol*. **1995**, *253*, 313–332.